LIMNOLOGY and OCEANOGRAPHY

ASLO

Limnol. Oceanogr. 70, 2025, 128–145

doi: 10.1002/lno.12746

Patterns of siderophore production and utilization at Station ALOHA from the surface to mesopelagic waters

Randelle M. Bundy,[1*] **Lauren E. Manck**,[2*] **Daniel J. Repeta**,[3] **Matthew J. Church**,[2] **Nicholas J. Hawco**,[4] **Rene M. Boiteau**,[5] **Jiwoon Park**,[1] **Edward F. DeLong**,[4] **Mak A. Saito**[3]

[1]School of Oceanography, University of Washington, Seattle, Washington, USA
[2]Flathead Lake Biological Station, University of Montana, Polson, Montana, USA
[3]Marine Chemistry and Geochemistry, Woods Hole Oceanographic Institution, Woods Hole, Massachusetts, USA
[4]Center for Microbial Oceanography Research and Education, University of Hawaii at Manoa, Honolulu, Hawaii, USA
[5]Department of Chemistry, University of Minnesota Twin Cities, Minneapolis, Minnesota, USA

Abstract

The North Pacific subtropical gyre is a globally important contributor to carbon uptake despite being a persistently oligotrophic ecosystem. Supply of the micronutrient iron to the upper ocean varies seasonally to episodically, and when coupled with rapid biological consumption, results in low iron concentrations. In this study, we examined changes in iron uptake rates, along with siderophore concentrations and biosynthesis potential at Station ALOHA across time (2013–2016) and depth (surface to 500 m) to observe changes in iron acquisition and internal cycling by the microbial community. The genetic potential for siderophore biosynthesis was widespread throughout the upper water column, and biosynthetic gene clusters peaked in spring and summer along with siderophore concentrations, suggesting changes in nutrient delivery, primary production, and carbon export seasonally impact iron acquisition. Dissolved iron turnover times, calculated from iron-amended experiments in surface (15 m) and mesopelagic (300 m) waters, ranged from 9 to 252 d. The shortest average turnover times at both depths were associated with inorganic iron additions (14 ± 9 d) and the longest with iron bound to strong siderophores (148 ± 225 d). Uptake rates of siderophore-bound iron were faster in mesopelagic waters than in the surface, leading to high Fe : C uptake ratios of heterotrophic bacteria in the upper mesopelagic. The rapid cycling and high demand for iron at 300 m suggest differences in microbial metabolism and iron acquisition in the mesopelagic compared to surface waters. Together, changes in siderophore production and consumption over the seasonal cycle suggest organic carbon availability impacts iron cycling at Station ALOHA.

Temporal range: 2013–2016.
Frequency or sampling interval: seasonal (monthly).
Spatial scale: site-based.

Oligotrophic subtropical gyres comprise the world's largest ocean biome (Longhurst 2010). Microbial communities inhabiting the oligotrophic ocean are exposed to low concentrations of nitrogen, phosphorus (Karl et al. 1997; Letelier et al. 2019), and dissolved iron (Fitzsimmons et al. 2015). Long-term studies by the Hawaii Ocean Time-series (HOT) at Station ALOHA in the North Pacific subtropical gyre demonstrate how seasonal to interannual-scale changes in nutrient supply can impact microbial communities and carbon export (Karl and Lukas 1996; Letelier et al. 2019). The resulting time series captures both the relatively stable conditions of the oligotrophic ocean and the importance of episodic and seasonal-scale delivery of nutrients to the upper ocean from storms, eddies, dust inputs, and the shoaling and deepening of the pycnocline (DiTullio and Laws 1991; Fitzsimmons et al. 2015; Hayes et al. 2015). Although this ecosystem is characterized by perennial nitrogen limitation, the microbial community of the euphotic zone is also consistently exposed to low dissolved iron concentrations, particularly in the deep chlorophyll maximum (Hawco et al. 2022; Hogle et al. 2022), and on sub-decadal timescales, the process of nitrogen fixation is thought to oscillate between phosphate and iron availability (Letelier et al. 2019).

*Correspondence: rbundy@uw.edu; lauren.manck@flbs.umt.edu

Additional Supporting Information may be found in the online version of this article.

Author Contribution Statement: RBundy and LEM wrote the manuscript and completed the analyses. RBoiteau and JP contributed data and edited the manuscript. EFD, MJC, NJH, MAS, and DJR helped design the study and edit the manuscript.
Randelle M. Bundy and Lauren E. Manck contributed equally to this work.

In seawater, the majority of dissolved iron (Fe) is complexed by a pool of organic ligands that have a high diversity of chemical structures. Complexation by organic ligands allows dissolved Fe to accumulate to concentrations above that set by its inorganic solubility (Gledhill and Buck 2012) and may help to retain Fe within the euphotic zone where it is needed to support primary production (Tortell et al. 1999). However, ligands significantly alter the bioavailability of the dissolved Fe pool by sequestering Fe in organic complexes, some of which require specific cellular transport systems in order to be accessed (Sutak et al. 2020). Changes in the external supply of Fe to the upper ocean at Station ALOHA have been shown to trigger organic ligand production on the timescale of days (Fitzsimmons et al. 2015).

Marine microorganisms, including both photoautotrophic and heterotrophic bacteria, have significant cellular Fe requirements and thus are equipped with molecular strategies for acquiring Fe from the Fe-scarce marine environment (Hopkinson et al. 2005; Sutak et al. 2020). A class of the strongest organic Fe-binding ligands, called siderophores, are secreted by marine bacteria and fungi in response to Fe deficiency as a high-affinity uptake strategy to solubilize and stabilize Fe in a molecular form that can be taken up by dedicated membrane transporters (Sandy and Butler 2009; Vraspir and Butler 2009). Many structurally diverse siderophores have been identified, and their biosynthesis pathways are categorized into two classes; non-ribosomal peptide synthetase (NRPS) pathways and NRPS-independent siderophore (NIS) synthetase pathways (Sandy and Butler 2009; Hider and Kong 2010). Siderophore biosynthesis is regulated by Fe concentrations in the surrounding environment, where elevated Fe suppresses synthesis (Sandy and Butler 2009). Some microbes can both synthesize and internalize Fe bound to siderophores, while others only possess outer membrane receptors for the uptake of exogenous siderophores that they cannot produce (Cordero et al. 2012; Kramer et al. 2020). Internalizing siderophore-bound Fe requires either cell surface receptors and transport pathways that are specific for certain siderophores or the ability to extracellularly reduce Fe(III) to Fe(II), releasing it from the siderophore complex; thus Fe complexed to siderophores has low bioavailability to the microbial community as whole (Shaked and Lis 2012), but is readily bioavailable to microbes that possess the relevant transport systems.

Dissolved siderophores represent 2%–10% of the total dissolved organic Fe-binding ligand pool present at Station ALOHA, and they likely play an important role in the competition for Fe and solubilization of Fe from particles (Bundy et al. 2018). North of Station ALOHA in the North Pacific transition zone, where Fe inputs from dust in the spring are elevated (Pinedo-González et al. 2020), siderophore concentrations and the transcription of siderophore biosynthesis and uptake genes are also elevated, further connecting the production of siderophores as a mechanism for solubilizing Fe from particles (Manck et al. 2022; Park et al. 2023). The metabolic potential for siderophore production and uptake is prevalent in the North Pacific subtropical gyre, transition zone, and the subpolar high nutrient low chlorophyll region (Hogle et al. 2022; Park et al. 2023). Although our understanding of the distributions of siderophores is improving, the environmental factors that trigger siderophore production in the ocean are not fully known. For example, despite siderophore synthesis being regulated by external Fe concentrations, they have been found in the ocean across both low and high Fe regions (Boiteau et al. 2016; Park et al. 2023).

Although the importance of siderophore production as a microbial Fe acquisition strategy in the marine environment has been recognized for some time (Mawji et al. 2008), little is known about their seasonal variability or turnover times. Understanding the biosynthesis and turnover times of siderophore-bound Fe will be important for interpreting their bioavailability and influence on Fe recycling and retention in the upper ocean over a variety of timescales. To address the gaps in our understanding of the timescales of siderophore cycling in the marine environment, we explored time and depth dependent changes in siderophore distributions, biosynthesis potential, and turnover times at Station ALOHA. Fe uptake rates and calculated turnover times of different Fe pools, together with the seasonal changes in siderophore biosynthesis, allow us to connect Fe cycling timescales to the seasonal cycle. By placing this study in the rich context of biogeochemical measurements made by the HOT program, we aim to better connect siderophore production and uptake to environmental conditions, to improve understanding of the impact of siderophores on microbial Fe acquisition and biogeochemical cycling in this important and well-studied oligotrophic ecosystem.

Methods

Radioactive iron uptake and siderophore bioavailability experiments

Fe uptake experiments were performed at Station ALOHA (Fig. 1a) at 15 and 300 m on two expeditions (HOT 278 in November 2015 and KM1605 in March 2016). Four treatments were used in all experiments: $FeCl_3$, ferrioxamine B, ferrioxamine E, and Fe-amphibactin. Note that when the $FeCl_3$ addition was added to natural seawater, it likely would immediately equilibrate with the natural organic ligands present and therefore is no longer purely $FeCl_3$, but this treatment is labeled as $FeCl_3$ for simplicity. Experiments at 15 m were performed both in the light and dark, and experiments at 300 m were performed only in the dark. Fe uptake was measured in two filter separated size fractions (> 2.0 and 0.2–2.0 μm) after 12 h. 500 nmol L^{-1} of nitrate was added to each of the 15 m experiments (Table S1) to alleviate nitrogen limitation control on Fe uptake. The results of the experiments were averaged across the two expeditions.

The isolation of amphibactin ligands used in this experiment has been described in detail elsewhere (Bundy

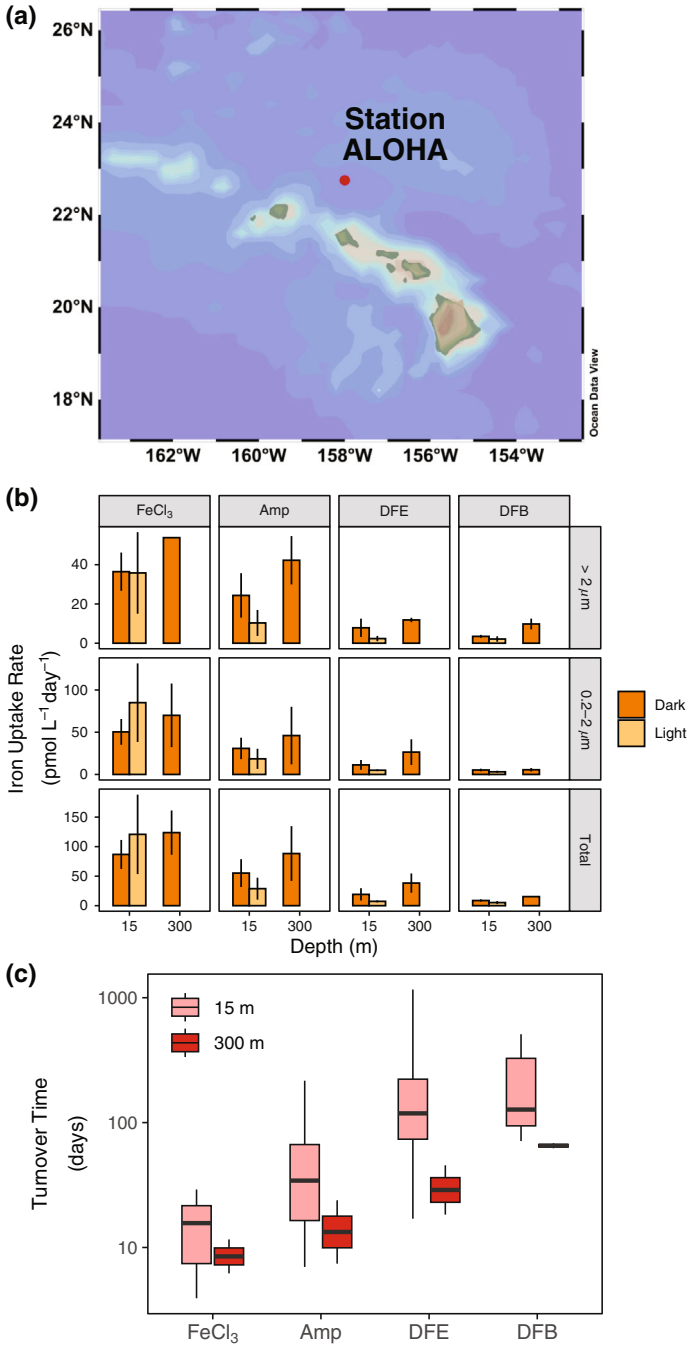

Fig. 1. (**a**) Map of the study region including the location of Station ALOHA (red dot). (**b**) Dissolved iron uptake rates (pmol L^{-1} d^{-1}) in the surface (15 m) and mesopelagic (300 m) at Station ALOHA after addition of 1 nmol L^{-1} iron as inorganic iron ($FeCl_3$) and iron bound to the siderophores amphibactin (Amp), ferrioxamine E (DFE), and ferrioxamine B (DFB). Dark and light measurements are displayed for both the 0.2–2.0 and > 2.0 μm size fraction. Total rates in the bottom panels represent the sum of both size fractions for each treatment. Mean values from all measurements for a given treatment are displayed and error bars represent the standard error of the mean. (**c**) Turnover time (days) of iron in each treatment at 15 and 300 m based on rates of total iron uptake in the dark. Box plots display the interquartile range with median values plotted as a solid horizontal line. The y-axis is on a $\log_{10}$ scale. Turnover times at 300 m were statistically different from 15 m only in the DFB treatment (pairwise *t*-test, $p < 0.05$).

et al. 2018), and the other ligand standards were commercially available. Radioactive Fe (^{55}Fe) ligand stocks were prepared using a 1 mCi ^{55}Fe stock (Perkin Elmer; Lot #091514) with a specific activity of 44.66 mCi mg^{-1} and an activity of 35.55 mCi mL^{-1}. Before making the ligand stocks, the concentration of the ^{55}Fe stock solution was calculated by converting the initial activity on the stock date to the current activity using the half-life of ^{55}Fe (2.73 years) and the number of days since the stock date. A primary ^{55}Fe stock of 55 μmol L^{-1} was used to prepare the ^{55}Fe-ligand and $^{55}FeCl_3$ stocks. The $FeCl_3$ stock was prepared in pH 2 (Optima HCl, Fisher Scientific) type I deionized water (MilliQ) while the siderophore stocks were prepared in type I deionized water. Ligand stocks were equilibrated for at least 24 h, but up to 5 d, before use, and ligands were present in three times excess of ^{55}Fe. Duplicate ligand stocks were made with the stable isotope ^{57}Fe (Cambridge Isotopes) to set up replicate treatments for cell counts that did not contain radioactivity.

Prior to beginning experiments at sea, quench curves were made to account for physical and chemical quench. Physical quench was accounted for by placing a blank filter in 10 mL of scintillation cocktail in triplicate and counting for 10 min on the liquid scintillation counter. Physical quench was also assessed by filtering a range of seawater volumes (10–500 mL) onto separate 0.2 μm filters containing no ^{55}Fe, and then placing each filter into 10 mL of scintillation cocktail and counting for 10 min. These physical quench controls account for whether the presence of cells or the filter itself impacts the counting efficiency of the liquid scintillation counter. The physical quench was found to be extremely small (< 1% of blanks), and for all further analyses, blank filters were used for quench correction. Chemical quench was assessed by setting up 10 separate vials of scintillation cocktail, each with the same activity of ^{55}Fe and increasing acetonitrile additions (0.1–10 nmol L^{-1}). The chemical quench was also found to be very small (< 5% of the blank) and was incorporated into the counting efficiency of the method for all samples.

To set up the incubation experiments, trace metal clean seawater collected from external spring Niskin bottles (X-Niskin) bottles (Ocean Test Equipment) from 15 and 300 m at sunrise and was dispensed into trace metal clean polycarbonate bottles. Four of the bottles were spiked with 1 nmol L^{-1} of the ^{57}Fe ligand stocks and the rest were spiked in duplicate with 1 nmol L^{-1} of the ^{55}Fe ligand stocks. A final concentration of 0.01% glutaraldehyde was added to four of the bottles to serve as "dead controls" and were incubated for 30 min before the experiment began to account for non-specific ^{55}Fe adsorption. All bottles were incubated in surface seawater flow-through incubators and dark treatments were double-bagged in black polyethylene bags. After 12 h (~ just after sunset), a flow cytometry sample was taken from each of the ^{57}Fe treatments and was preserved with 0.01% glutaraldehyde for 30 min before being flash-frozen in liquid nitrogen and stored at −80°C. At the end of the 12 h experiment, each bottle was sequentially filtered onto acid washed 2.0 and

0.2 μm filters using low pressure vacuum filtration to distinguish uptake by picoplankton (0.2–2.0 μm) from larger nanoplankton or particle-associated organisms (> 2.0 μm). Both filters were washed three times with an oxalate wash to remove extracellular Fe (Tovar-Sanchez 2003).

A key assumption of these experiments is that all Fe remains complexed to the respective added siderophore throughout the duration of the experiment (12 h). To confirm this was the case, the remainder of the treatments spiked with the ^{57}Fe-siderophore stocks were filtered with a 0.2 μm polycarbonate filter, and the filtrate was pre-concentrated onto a solid phase extraction column (Bond Elut ENV, Agilent Technologies) and were treated and analyzed in the same manner as the dissolved siderophore samples from the water column as described below. ^{57}Fe peaks from liquid chromatography inductively coupled plasma mass spectrometry analyses were examined to determine whether any free ^{57}Fe not associated with each of the added siderophores was present. No significant free ^{57}Fe was observed in these treatments, confirming the full complexation of each ligand in the siderophore treatments (data not shown).

Radioactive decay on each filter and in each treatment was determined using a liquid scintillation counter (Beckman-Coulter LS6500). ^{55}Fe disintegrations per minute (dpm) were background and dead control corrected and converted to a concentration of Fe uptake using a standard curve. Fe uptake rates were then calculated based on the total amount of Fe that was incorporated into biomass onto each filter size fraction and in each treatment. Total Fe uptake over the 12-h incubation was converted to total Fe uptake per day (over 24 h). We then estimated Fe uptake rates for heterotrophic bacteria specifically, which we assumed to be the dominant community responsible for any observed Fe uptake in the dark (Table S1). The Fe uptake per cell per day (amol Fe cell^{-1} d^{-1}) was estimated using flow cytometry cell counts of heterotrophic bacteria in the ^{57}Fe treatments (Bundy et al. 2018) and the total Fe uptake in the dark (Table S1). Fe : C ratios (μmol : mol) for heterotrophic bacteria were calculated using a carbon quota of 12.4 fg C cell^{-1} (Strzepek et al. 2005; Boyd et al. 2015) and assuming a growth rate of 1 d^{-1} (Jones et al. 1996; Table S1). As an additional constraint on Fe : C per cell, Fe uptake rates were compared to average rates of bacterial carbon production measured at or near Station ALOHA, 23 ± 8 nmol C L^{-1} d^{-1} and 0.9 ± 1.3 nmol C L^{-1} d^{-1} at 5 and 300 m, respectively. The rate of bacterial production at 5 m is an average value of those measured at Station ALOHA (Viviani and Church 2017). The mean rate at 300 m was calculated from measurements conducted on three cruises near Station ALOHA in the North Pacific subtropical gyre (KOK1507, KM1605, and KM1709). All data are publicly available on the Simons Collaborative Marine Atlas Project. In each case, leucine incorporation was measured using the methods described by Smith and Azam (1992) and a conversion factor of 1.5 kg C mol^{-1} leucine was used to convert leucine incorporation to bacterial carbon production.

In addition to Fe uptake rates, the turnover rate of Fe in each treatment was calculated based on,

$$\text{Turnover rate} = \frac{\text{Total iron uptake rate}}{\text{Total iron}} \quad (1)$$

where the total Fe uptake rate (pmol L^{-1} d^{-1}) is the sum of the radioactive Fe uptake in both size fractions and the total Fe is the radioactive Fe added (1 nmol L^{-1}) plus the in situ dissolved Fe concentration (Bundy et al. 2018). The turnover time of Fe (in days) for each treatment was calculated as 1 divided by the turnover rate.

Contextual environmental properties

Data for concentrations of nitrate + nitrite ($NO_3^- + NO_2^-$), chlorophyll *a* (chl *a*), rates of primary production, and carbon flux at Station ALOHA were accessed for the study period January 1, 2013 to December 31, 2016. All data are publicly available via the HOT-Data Organization and Graphical System. Primary production is routinely estimated based on assimilation of ^{14}C by the HOT program at depths of 5, 25, 45, 75, 100, and 125 m (Karl et al. 2021). Particulate carbon flux is measured from sediment traps at 150 m. Additional details on the sampling strategies used by the HOT program can be found elsewhere (Karl and Lukas 1996) and the analytical methods used for HOT measurements can be found online (https://hahana.soest.hawaii.edu/hot/methods/results.html). $NO_3^- + NO_2^-$ concentrations were determined using the high-sensitivity chemiluminescent method (Dore and Karl 1996; Foreman et al. 2016). Depth integrated (0–150 m) fluxes and stocks were calculated using trapezoidal approximations, assuming homogenous mixing between 0 and 5 m. To integrate rates of primary production to 150 m, monthly mean rates measured at 150 m during the first 12 years of the HOT program (Karl et al. 2021) were added to the 0–125 m integrated value calculated during this study period. The *e*-ratio for each HOT cruise during the study period was calculated as the rate of particulate carbon flux measured at 150 m divided by the depth integrated (0–150 m) rate of primary production.

Because samples for dissolved Fe (< 0.2 μm) concentrations are not routinely measured by the HOT program, measurements made from previous studies at Station ALOHA (Fitzsimmons et al. 2015; Bundy et al. 2018) were used for context. These measurements largely fall within the spring and summer months. Therefore, to visualize potential seasonal changes in dissolved Fe concentrations, 3-day average dissolved Fe concentrations at Station ALOHA during the study period were obtained from the MIT Darwin model (Dutkiewicz et al. 2015) via the Simons Collaborative Marine Atlas Project (CMAP): https://simonscmap.com/catalog/datasets/Darwin_Nutrient. Seasons were defined in this study as—Winter: December, January, February; Spring: March, April, May; Summer: June, July August; Fall: September, October, November. Additionally, vertical regions were defined here as: upper euphotic zone: ≤ 75 m; lower euphotic zone: > 75

to ≤ 150 m; upper mesopelagic zone: > 150 to ≤ 300 m; mid-mesopelagic zone: > 300 to ≤ 500 m.

Siderophore collection and analyses

Dissolved siderophore samples were collected on six cruises from 2013 to 2016, each within 100 km of Station ALOHA (Table S2). Samples were collected via Teflon diaphragm pump or 8 L X-Niskin bottles on a trace metal rosette using a non-metallic line. Samples were filtered (0.2 μm Acropak 200 or Pall capsule) into acid-cleaned fluorinated high-density polyethene 200 L barrels (expeditions from 2013 to 2014; Boiteau et al. 2013) or 20 L carboys (all other expeditions; Bundy et al. 2018). For each sample collected in 2013 and 2014, 20–800 L of filtered seawater was preconcentrated, and for all other samples 15–20 L of filtered seawater was collected. Filtered samples were preconcentrated at a flow rate of 15–18 mL min^{-1} onto 1000 mg solid phase extraction columns containing (Bond Elut ENV, Agilent Technologies). After preconcentration, each column was flushed with three column volumes of trace metal clean type I deionized water until dry and then was stored at − 20°C until analysis.

Solid phase extraction columns were slowly thawed in the dark and then eluted with three column volumes of distilled or Optima grade methanol (Fisher Scientific). Methanol extracts were dried to approximately 0.5–1 mL using a SpeedVac (Thermo Fisher). Either 25 or 50 μL of the extract was first injected into a PEEK-lined C8 column and compounds were separated using liquid chromatography (LC) on a Dionex 3000 high pressure liquid chromatography (HPLC) system. Details on the chromatography are presented in Boiteau et al. (2016) and Bundy et al. (2018). Briefly, compounds were separated using a 20 min gradient of 95% solvent A/5% solvent B to 10% solvent A/90% solvent B (solvent A = 5 mM ammonium formate in type I deionized water, solvent B = 5 mM ammonium formate in distilled methanol), followed by a step from 90% to 95% solvent B (Boiteau et al. 2016; Bundy et al. 2018). Fe-bound compounds eluted from the column were monitored by inductively-coupled plasma mass spectrometry on an iCap-Q (Thermo Scientific). The sample was introduced at a flow rate of approximately 50 μL min^{-1} and oxygen add gas was introduced at a flow rate of approximately 25 mL min^{-1} to minimize the deposition of reduced carbon on the cones. The inductively-coupled plasma mass spectrometer was equipped with a perfluoroalkoxy micronebulizer (PFA-ST; Elemental Scientific), platinum sampler and skimmer cones, and a cyclonic spray chamber cooled to 0°C. Counts per second of ^{56}Fe, ^{57}Fe, ^{54}Fe, and ^{59}Co were monitored in kinetic energy discrimination mode (KED) and distinct peaks in ^{56}Fe and ^{57}Fe were integrated using in-house R scripts. Peak areas were converted to concentration using a four-point standard curve with ferrioxamine E, and were corrected for sensitivity changes throughout the run using the peak area of ^{59}Co from a cyanocobalamin internal standard. All distinct quantifiable Fe peaks were categorized as putative siderophores and the concentrations of these peaks were summed for each sample to give a total siderophore concentration (Table S2).

To identify the putative siderophores, samples were then analyzed using liquid chromatography coupled to electrospray ionization mass spectrometry on an Orbitrap Fusion (Thermo Scientific). The same chromatography was used, and the inductively coupled plasma mass spectrometry and electrospray ionization mass spectrometry data were aligned based on the retention time of the ^{59}Co peak from cyanocobalamin in the inductively coupled plasma mass spectrometry trace and the presence of the cyanocobalamin m/z in the electrospray ionization mass spectrometry data ($m/z = 678$). Putative siderophores were identified using a targeted search of the MS^1 m/z based on a database of known siderophores (Baars et al. 2014). Fragmentation data (MS^2) was then examined and compared to literature values or in silico fragmentation prediction (CFM-ID 3.0), and siderophores that had a matching MS^2 fragment to literature values or in silico prediction were assigned a structural identification (Table S2).

Siderophore biosynthetic gene cluster analysis

Details on the sampling, processing and data analyses of metagenomes collected at Station ALOHA are presented elsewhere (Mende et al. 2017; Luo et al. 2020). The ALOHA gene catalog consists of ~ 8.9 million non-redundant genes detected from concentrated plankton biomass (size fractionated to 0.22–1.6 μm) collected between the surface and 1000 m over ~ 1.5 years at near monthly frequency (Mende et al. 2017). To identify putative siderophore biosynthetic gene clusters within the ALOHA gene catalog, biomarker genes for both NRPS pathways and NIS pathways were first identified. To identify NIS pathways in the ALOHA gene catalog, hidden Markov models for the conserved domains pfam04183 (IucA/IucC siderophore synthases) and pfam06276 (FhuF-like reductases) were searched for in the ALOHA gene catalog using HMMER (Eddy 2011) which resulted in the detection of 20 NIS homologs (Table S3). NIS pathways are specific to siderophore biosynthesis, hence the 20 identified NIS homologs could be confidently attributed to siderophore biosynthesis. For NRPS biosynthetic pathways, we searched for the conserved domain pfam00501, an AMP-binding domain inclusive of the adenylation domain of NRPS modules. The resulting 28,000+ genes were then screened with antiSMASH (Medema et al. 2011) to determine the presence of a complete or near-complete NRPS module with adenylation, peptidyl carrier protein (pfam00550), and condensation (pfam00668) domains. This resulted in the detection of 132 NRPS homologs. Because NRPS biosynthetic pathways are not unique to siderophore biosynthesis, further examination of the identified NRPS homologs was required. Each NRPS homolog, along with neighboring genes from the ALOHA gene catalog contig assembly, were analyzed using the predictive tools within the antibiotics and Secondary Metabolite

Analysis Shell (antiSMASH) pipeline with default parameters for the relaxed detection strictness setting. In addition to the default features, Minimum Information about a Biosynthetic Gene (MIBiG) cluster comparison and Cluster pfam analysis were also performed. This enabled predictions of the amino acid specificity for each adenylation domain within the NRPS modules, detection of additional conserved domains, and Basic Local Alignment Search Tool (BLAST) comparisons to characterized biosynthetic gene clusters. This resulted in the putative identification of 18 NRPS pathways for the biosynthesis of siderophores from the ALOHA gene catalog (Table S3). Combined, a total of 38 putative siderophore biosynthetic gene clusters consisting of 101 unique genes were identified and used for downstream analysis (Table S3). The antiSMASH pipeline was utilized to assign putative structural characterizations to these siderophore biosynthetic gene clusters based on comparisons to known biosynthetic pathways. We note that while this is a conservative approach to identifying siderophore biosynthetic gene clusters that may exclude siderophores without well-characterized biosynthetic pathways, it has resulted in a list of genes with high percent identity to known siderophore biosynthesis genes, giving us confidence in the functional annotation of genes used for downstream analysis.

To examine the distribution of siderophore biosynthetic gene clusters with depth and across time at Station ALOHA, metagenomic sequence reads from plankton biomass (> 0.2 μm) collected on HOT cruises between May 2015 and April 2016 (NCBI BioProject PRJNA352737) were mapped to open reading frames of the ALOHA gene catalog. The terms open reading frame and gene will be used interchangeably throughout the text. In total, this consisted of 132 samples from 5 to 500 m, spanning 11 months. Forward and reverse reads from each sample were quality trimmed with Trimmomatic (Bolger et al. 2014) and mapped to the ALOHA gene catalog using Burrows-Wheeler Aligner (Li and Durbin 2009) with a 95% nucleotide identity threshold and minimum alignment length of 45 bp. Reads aligned as proper pairs were then counted with FeatureCounts (Liao et al. 2014) and multiple mappers were fractionally distributed. Finally, read counts were normalized to reads per kilobase per million for further analysis. Reads from the 2015–2016 dataset recruited to 24 of the 38 siderophore biosynthetic gene clusters identified in the ALOHA gene catalog (Table S3).

Results

Uptake and turnover time of siderophore-bound iron by the microbial community

The relevant timescales of siderophore cycling were assessed in several ways in this study. Uptake experiments were used to quantify Fe uptake rates when bound to different siderophores, and these results were related to siderophore seasonal distributions. Uptake rates of inorganic Fe additions were the highest across all treatments (Fig. 1b; Table S1). The inorganic Fe treatments likely represented $FeCl_3$ that associated with unbound natural ligands present in excess of the in situ dissolved Fe in the experiment (Bundy et al. 2018). Uptake rates of $FeCl_3$ at both 15 and 300 m were higher on average in the 0.2–2.0 μm size fraction compared to the > 2.0 μm size fraction. In the > 2.0 μm size fraction, uptake rates of $FeCl_3$ at 15 m were comparable in the light and the dark ($\sim$ 36 pmol L^{-1} d^{-1}). In contrast, $FeCl_3$ uptake was higher (on average) in the light (85 pmol L^{-1} d^{-1}) compared to the dark (50 pmol L^{-1} d^{-1}) in the 0.2–2.0 μm size fraction (Fig. 1b).

Siderophore-bound Fe was readily accessible by the microbial community at 15 and 300 m at Station ALOHA (Fig. 1b; Table S1). The relative uptake rate varied for the different Fe-siderophore treatments. At both depths, the Fe-amphibactin amendment was taken up the fastest (54 pmol L^{-1} d^{-1}), followed by ferrioxamine E (19 pmol L^{-1} d^{-1}) and ferrioxamine B (9 pmol L^{-1} d^{-1}). In contrast to $FeCl_3$, the uptake rate of siderophore-bound Fe was generally higher in the dark (33 pmol L^{-1} d^{-1}) compared to the light (14 pmol L^{-1} d^{-1}). Similar to the $FeCl_3$ treatment, Fe uptake was higher on average in the 0.2–2.0 μm fraction compared to the > 2.0 μm fraction across all siderophore treatments (Fig. 1b).

Surprisingly, the uptake rate of siderophore-bound Fe was higher at 300 m compared to 15 m leading to shorter Fe turnover times (Fig. 1c). In general, at both 15 and 300 m the turnover times were shortest in $FeCl_3$ treatments, followed by Fe bound to amphibactins, ferrioxamine E and ferrioxamine B. The average turnover time of Fe at 15 m ranged from 15 $\pm$ 8 d in the $FeCl_3$ treatment to 252 $\pm$ 376 and 215 $\pm$ 165 d in the ferrioxamine E and ferrioxamine B treatments, respectively. Mean turnover times at 300 m ranged from 9 $\pm$ 4 d in the $FeCl_3$ treatment to 65 $\pm$ 4 d in the ferrioxamine B treatment (Fig. 1c). Across all treatments, turnover times of Fe were consistently shorter at 300 m compared to 15 m (Fig. 1c), though this difference was only significant in the ferrioxamine B treatment (pairwise *t*-test, $p < 0.05$).

The Fe uptake per cell (amol Fe day^{-1} $cell^{-1}$) was calculated from the total Fe uptake rate. The Fe uptake rates in the dark from the 0.2–2.0 and > 2.0 μm size fractions were summed for a given Fe substrate (Table S1) and normalized to the abundance of heterotrophic bacteria measured via flow cytometry, assuming that the Fe uptake in the dark treatments was dominated by these organisms. This is likely a valid assumption for the experiments done at 300 m, but for experiments done at 15 m there could be additional Fe uptake in the dark by phytoplankton. The resulting Fe uptake per cell at 15 m ranged from 0.01 to 0.14 amol Fe $cell^{-1}$ d^{-1}, increasing to 0.18–1.46 amol Fe $cell^{-1}$ d^{-1} at 300 m given the higher total rates of Fe uptake and much lower cell abundances (Table S1).

Cellular Fe : C ratios were calculated in two different ways (*see* section Contextual environmental properties). We determined an Fe quota per cell (pmol Fe $cell^{-1}$) at the end of each experiment assuming a bacterial growth rate of 1 d^{-1} (Jones

et al. 1996), such that the Fe uptake rate per cell is equal to the cellular Fe quota. These cellular Fe quotas were then converted to Fe : C ratios using a fixed carbon quota of 12.4 fg C $cell^{-1}$ (Strzepek et al. 2005; Boyd et al. 2015). The second method compared total Fe uptake rates (pmol Fe L^{-1} d^{-1}) to average rates of bacterial carbon production measured at or near Station ALOHA based on leucine incorporation (23 and 0.9 nmol C L^{-1} d^{-1} at 15 and 300 m, respectively). This represents the ratio at which Fe and carbon are actively being acquired by bacterial cells and does not require assumptions of growth rates or cellular carbon quotas, but does presume a constant leucine : carbon ratio within biomass. While both of these methods are limited by the reliance on available conversion factors for determining cellular carbon content, they can provide useful insight on the range of the cellular Fe : C ratio of heterotrophic bacteria under varying conditions. At 15 m, the Fe : C per cell calculated using a fixed carbon quota ranged from $6.8 \pm 3.5\,\mu$mol : mol (ferrioxamine B treatment) to $68 \pm 43\,\mu$mol : mol ($FeCl_3$ treatment; Table S1). In contrast, the Fe : C calculated using average rates of bacterial production ranged from $380 \pm 192\,\mu$mol : mol to $3775 \pm 2386\,\mu$mol : mol (Table S1). We note that by assuming a lower heterotrophic bacterial growth rate of $0.05\,d^{-1}$ in surface waters (Kirchman 2016), and using a fixed carbon quota, increases the Fe : C ratios determined by the first method, reducing the discrepancy between the two approaches. Likewise, assuming a lower carbon quota per cell further increases the Fe : C ratio (by as much as twofold). We chose to keep the estimates using a growth rate of $1\,d^{-1}$ as our lower bound since these estimates are comparable to Fe : C values reported previously (Tortell et al. 1999). Irrespective of which approach was used, the Fe : C per cell was higher at 300 m than 15 m. The Fe : C per cell calculated from a fixed carbon ratio at 300 m ranged from $88 \pm 6\,\mu$mol : mol (ferrioxamine B treatment) to $711 \pm 305\,\mu$mol : mol ($FeCl_3$) treatment, while Fe : C per cell based on bacterial production ranged from $17{,}044 \pm 1131$ to $137{,}500 \pm 58{,}941\,\mu$mol : mol in the ferrioxamine B and $FeCl_3$ treatments, respectively (Table S1). These high Fe uptake rates were observed even after oxalate washing to remove adsorbed Fe and subtraction of a dead control, indicating that they do reflect internalization and uptake of Fe and not, for example, surface adsorption or authigenic Fe-oxide precipitation.

Seasonal changes in nutrients and productivity at station ALOHA during the study period

Fe uptake rates and seasonal siderophore distributions were assessed in the context of Station ALOHA, a well-studied oligotrophic time-series station in the North Pacific that is sampled by the HOT program on a nearly monthly basis (Fig. 1a). This region is characterized by low surface nutrient concentrations and a persistent deep chlorophyll maximum centered around 100 m (Fig. 2a). During the study period, monthly mean nitrate + nitrite concentrations in the upper euphotic zone ranged from 1.4 ± 0.4 nmol L^{-1} in August to 5.7 ± 0.8 nmol L^{-1} in November (Figs. 2b, S1A). Below 100 m, nitrate + nitrite concentrations increased rapidly and were more variable than the upper euphotic zone. Between 100 and 150 m, monthly mean nitrate + nitrite concentrations during the study period reached minimum values in May (269.8 ± 274.6 nmol L^{-1}) and maximum values in August (1967.3 ± 1858.3 nmol L^{-1}; Figs. 2b, S1B). High variability in nitrate + nitrite in August stemmed in part from a period of negative sea level anomalies present at Station ALOHA during August 2015; isopycnal uplift associated with the passage of a cyclonic eddy increased nutrient concentrations in the lower euphotic zone. Mean monthly depth integrated stocks of nitrate + nitrite (mmol N m^{-2}) in the upper and lower euphotic zone followed similar monthly patterns to that of average $NO_3^- + NO_2^-$ concentrations (Fig. S2).

Dissolved Fe concentrations are persistently low (< 0.5 nmol Fe L^{-1}) in surface waters at Station ALOHA. Since dissolved Fe data were limited during the study period, 3-day averaged dissolved Fe concentrations generated from the MIT-Darwin model were used as a potential means to explore seasonal variation in dissolved Fe concentrations, despite the known limitations of modeling dissolved Fe (Tagliabue et al. 2016). Model output predicted minimum concentrations of dissolved Fe in the upper euphotic zone with low seasonal variability (Fig. 2c). However, dissolved Fe measurements collected during spring and summer months between 2012 and 2015 at Station ALOHA suggested dissolved Fe concentrations of the upper euphotic zone varied as much as 10-fold (0.08–0.87 nmol L^{-1}), variability that is not captured in the model output (Fig. 2c). This high degree of variability in the upper euphotic zone is likely a result of episodic atmospheric dust deposition which can impact dissolved Fe concentrations in the upper euphotic zone (Fitzsimmons et al. 2015). Given the lack of agreement between model output and observations during the spring and summer in the upper euphotic zone, dissolved Fe availability in this region of the water column during fall and winter remains unconstrained without further measurements. Both model and observational data suggested consistently low (≤ 0.1 nmol L^{-1}) dissolved Fe concentrations between 100 and 125 m, corresponding with the typical depth of the deep chlorophyll maximum. Below 125 m, dissolved Fe concentrations began to increase. However, the observational data suggest there is a deeper fericline than that indicated by model output.

Mean monthly rates of primary production in the upper euphotic zone peaked in October (7.8 ± 2.4 mg C m^{-3} d^{-1}) and were the lowest in February (4.8 ± 1.9 mg C m^{-3} d^{-1}; Fig. S1A). Between 100 and 150 m, mean monthly rates of primary production peaked in July (4.2 ± 0.8 mg C m^{-3} d^{-1}) with minimum values observed in December (1.1 ± 0.3 mg C m^{-3} d^{-1}; Fig. S1B). Depth integrated rates of primary production (0–150 m) increased from winter to summer before decreasing in fall (Fig. 3a). Maximum monthly mean values were observed in June (728.8 ± 87.6 mg C m^{-2} d^{-1}) and minimum values in December (453.4 ± 23.0 mg C m^{-2} d^{-1}). The particulate carbon flux at 150 m during the same time period showed similar

monthly patterns to primary production (Fig. 3b), but with relatively high fluxes observed during January and February. As a result, relatively small changes in the monthly mean *e*-ratio (the ratio of sinking particulate carbon flux at 150 m relative to euphotic zone primary production) were detected, but followed similar patterns to those of particulate carbon flux (Fig. 3c). The highest monthly mean values were observed in February (0.062 ± 0.031) and August (0.058 ± 0.021) with the lowest in December (0.030 ± 0.009). The average C : N ratio of the particulate flux at 150 m increased over the summer months from 6.8 ± 0.3 in April to 8.4 ± 1.2 in August, indicating that carbon-enriched particulate matter contributed to periods of high and relatively efficient export. However, the overall low *e*-ratios observed across the study period are consistent with intense remineralization of organic matter within the euphotic zone. Seasonal patterns in productivity observed during the 2013–2016 study period discussed here are consistent with those observed across the entire 30 year period of the HOT program (Karl et al. 2021).

Seasonal distribution of siderophores and siderophore biosynthesis genes at station ALOHA

To connect the turnover time of Fe bound to siderophores to the environmental distributions of these compounds, we examined both dissolved siderophore concentrations and the abundance of siderophore biosynthesis genes. Dissolved

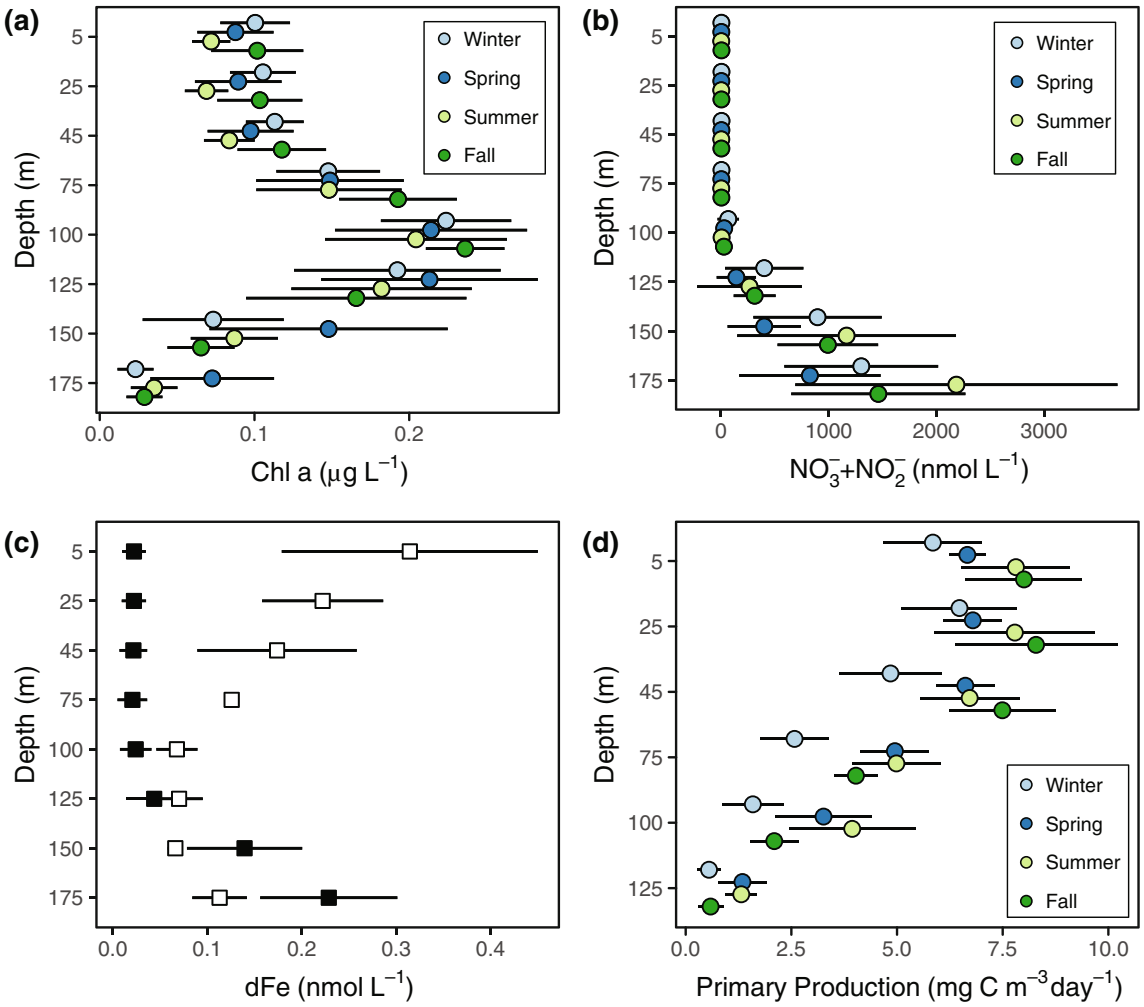

Fig. 2. Depth profiles of (**a**) chlorophyll *a* (Chl *a*) concentrations (μg L^{-1}), (**b**) nitrate + nitrite ($NO_3^- + NO_2^-$) concentrations (nmol L^{-1}), (**c**) dissolved iron (dFe) concentrations (nmol L^{-1}), and (**d**) rates of primary production (mg C m^{-3} d^{-1}) during the 2013–2016 study period at Station ALOHA. Depth profiles in a–c display the mean concentrations at each depth for a given season and error bars represent the standard deviation from the mean. Depth profiles in c display the mean dissolved Fe concentrations at each depth across the entire study period for available in situ measurements (open squares) and model output from the MIT Darwin model (closed squares) and error bars represent the standard deviation from the mean.

siderophore concentrations and the abundance of siderophore biosynthetic gene clusters changed seasonally at Station ALOHA as well as with depth (Figs. 4, 5). Total dissolved siderophore concentrations varied from undetectable to 95.3 pmol L^{-1} during the entire study period. Note that in the fall, siderophore concentrations were only measured at 15 m, limiting assessment of seasonality in siderophore concentrations in the mesopelagic waters during this season. Average siderophore concentrations throughout the whole water column were highest in the spring (21.8 ± 41.5 pmol L^{-1}), fall (8.4 ± 8.1 pmol L^{-1}), and summer (3.0 ± 4.2 pmol L^{-1}) and lower in winter (0.4 ± 0.6 pmol L^{-1}; Fig. 5). However, high variability was observed in each depth range within a season. In the upper euphotic zone where most samples were collected, siderophore concentrations were highest on average in the spring (47.8 ± 67.2 pmol L^{-1}), fall (8.4 ± 8.1 pmol L^{-1}), and summer (2.4 ± 0.1 pmol L^{-1}), followed by winter (0.4 ± 0.3 pmol L^{-1}; Fig. 4; Table S2).

The capacity for siderophore production as indicated by the presence of genes from siderophore biosynthetic gene clusters was detected at Station ALOHA across all seasons and at all depths sampled during the study period (Fig. 5a; Table S3). Similar to dissolved siderophore concentrations, genes from siderophore biosynthetic gene clusters also showed low and relatively uniform abundances (< 0.2 reads per kilobase per million) in the winter in both the euphotic and mesopelagic zones, increasing in the euphotic zone in the spring and summer (Fig. 5b). Monthly median gene abundances in the euphotic zone peaked during the summer (July, 0.30 reads per kilobase per million), decreasing throughout the fall in the upper euphotic zone, but remaining elevated in the lower euphotic zone. The lowest monthly median gene abundances in the euphotic zone were observed in January and February (0.04 reads per kilobase per million). Mesopelagic gene abundances were less seasonally variable (Fig. 5b), with median gene abundances ranging 0.05–0.11 reads per kilobase per million. Monthly median gene abundances were maximal in April (0.15 reads per kilobase per million) and genes from siderophore biosynthetic gene clusters were not detected in October in the mesopelagic.

Several different siderophores were detected both as dissolved siderophores in the water column and as a biosynthetic gene clusters in the Station ALOHA gene catalog (Table 1). Of those identified in the water column, primarily hydroxamate or mixed siderophores were detected, with ferrioxamines and amphibactins being the most common (Table 1). The detected siderophore biosynthetic gene clusters largely belonged to catecholate, carboxylate and mixed siderophores (Table 1). Two ferrioxamine biosynthetic gene clusters were identified in the ALOHA gene catalog, however, these biosynthetic gene clusters were not detected in the 2015–2016 metagenomic dataset. Several siderophores were found both in the water column and in the metagenomes, including petrobactin, pseudoalterobactin, piscibactin and vibrioferrin (Table 1). The biosynthesis genes were primarily homologs of known genes from *Vibrio*, *Photobacterium*, *Alteromonas*, and *Pseudoalteromonas* (Table S3).

Discussion

Turnover times of inorganic iron and iron-siderophore complexes reflect bioavailability to the microbial community

Siderophore-mediated acquisition of dissolved Fe involves secretion, uptake, and recycling of these compounds, and the turnover time of each Fe source reflects its bioavailability. In this study, the turnover times of siderophore-bound Fe were assessed to connect the seasonal distributions of siderophores with estimates of their lifetimes in the marine environment. Siderophore-bound Fe was taken up less rapidly than the inorganic Fe additions. Siderophore Fe uptake had average turnover times ranging from 15 to 250 d (Fig. 1c) and an average turnover time of 148 d from all depths and siderophore treatments, while $FeCl_3$ turned over more rapidly averaging 14 d (Fig. 1c). The different turnover times reflects differences in the bioavailability of inorganic vs. organically-bound Fe (Lis et al. 2015). The average turnover times of $FeCl_3$ observed in this study were very similar to turnover times of 14–18 d in the mixed layer during June 2019, measured at near-background dissolved Fe concentrations at Station ALOHA (Hawco et al. 2022). The turnover times calculated here could also be impacted by possible wall adsorption of the ^{55}Fe spike during the incubation experiment, but we expect this to be minimal during the short duration of the incubations. It is also important to note that these turnover times are based only on Fe uptake rates, and do not include impacts from other processes such as grazing of bacteria during the incubation or photodegradation of organic ligands. The shorter turnover of $FeCl_3$ likely reflects weaker binding of inorganic Fe associated with ligands naturally present in seawater, which are more accessible to phytoplankton using ferric reductases as an uptake mechanism (Maldonado and Price 2001; Salmon et al. 2006; Lis et al. 2015).

The Fe uptake rates varied by Fe source and were within ranges observed in other studies (Fourquez et al. 2020; Lory et al. 2022). We found rates of $FeCl_3$ uptake were higher in the light than in the dark, suggesting photoautotrophic uptake may be substantial. Uptake rates of siderophore-bound Fe, in contrast, were always higher in the dark than the light, suggesting that siderophore iron consumption was likely controlled by chemotrophic plankton and that photochemical impacts on the uptake of siderophore-bound Fe were minimal (Barbeau 2006). We were not able to distinguish Fe uptake by specific microbial populations in this study (e.g., *Prochlorococcus*; Lory et al. 2022), so these assumptions are based on which populations are most likely to dominate in the light vs. dark treatments. Regardless, the turnover time of Fe bound to siderophores was much longer, on the order of weeks to months,

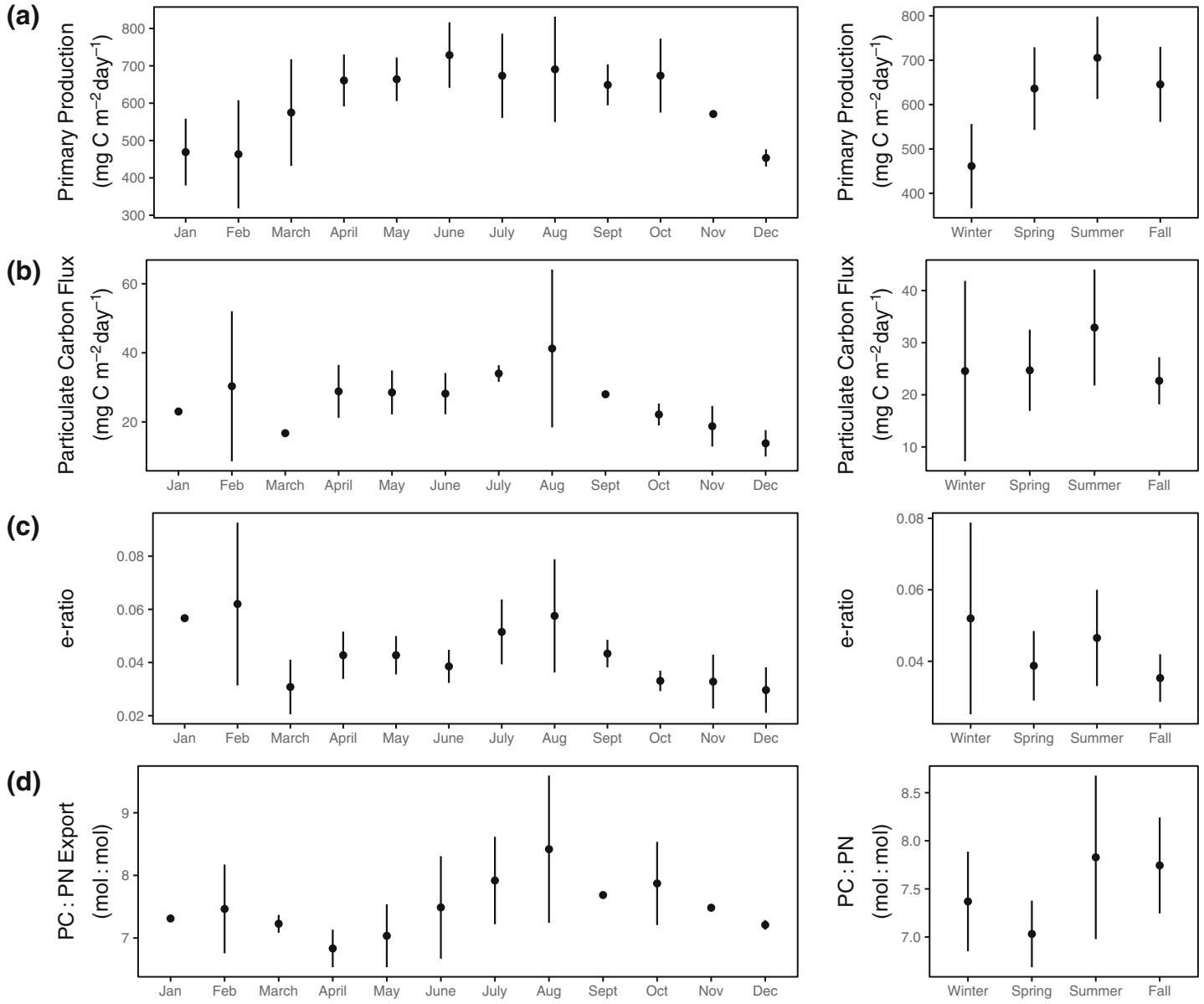

Fig. 3. Monthly and seasonal mean values of (**a**) depth-integrated rates of primary production (mg C m^{-2} d^{-1}) from 0 to 150 m, (**b**) particulate carbon flux (mg C m^{-2} d^{-1}) at 150 m, (**c**) the *e*-ratio defined as the proportion of particulate carbon flux at 150 m compared to the 0–150 m depth-integrated rate of primary production, and (**d**) the C : N ratio of sinking particulate matter collected at 150 m at Station ALOHA during the 2013–2016 study period. Error bars represent the standard deviation from the mean.

suggesting that Fe bound to siderophores is longer-lived than the inorganic and/or weakly bound Fe pool, and may help to retain dissolved Fe in both euphotic and upper mesopelagic waters.

Turnover times of siderophore-bound Fe varied depending on the siderophore. Fe associated with amphibactins was taken up more quickly than ferrioxamine E or B (Fig. 1b). Amphibactins have a lower binding affinity to dissolved Fe (log of the conditional stability constants = 12.0–12.5; Bundy et al. 2018) compared to ferrioxamines (log of the conditional stability constants = 14.0–14.4; Bundy et al. 2018), and therefore Fe could be more easily reducible from amphibactins. Alternatively, more members of the microbial community may possess direct Fe-amphibactin uptake pathways, but these uptake pathways are not well-constrained (Boiteau et al. 2016). The relative turnover times and bioavailability of the different siderophores, therefore, appeared to be governed by their binding strengths in this case. In our experiments, the highest uptake rates of siderophore-bound Fe were also found in the 0.2–2.0 μm size fraction and in the dark, suggesting Fe bound to siderophores may be more accessible to heterotrophic

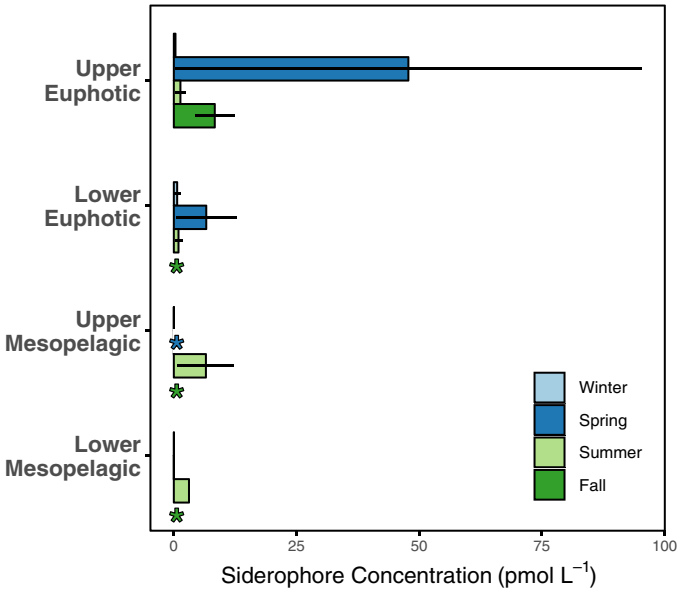

Fig. 4. Seasonality in dissolved siderophore concentrations (pmol L^{-1}) at Station ALOHA between 2013 and 2016. Bars display the mean values of measurements collected within the same depth range for a given season and error bars, when present, represent the standard error of the mean. Asterisks indicate when no data are present for a given depth range and season. Depth ranges are as follows: upper euphotic 0–75 m, lower euphotic > 75 and ≤ 150 m, upper mesopelagic > 150 and ≤ 300 m, mid-mesopelagic > 300 and ≤ 500 m.

bacteria rather than larger photoautotrophs, who were more likely to dominate the Fe uptake in the light treatments.

Rates of iron acquisition by the microbial community are elevated in the mesopelagic waters of station ALOHA relative to the euphotic zone

The uptake rates of Fe and the distribution of siderophores bound to iron varied both with season and depth, indicating a possible connection between the turnover times of Fe pools and vertical and time-varying changes in primary production and particle export. An unexpected result of this work was the faster uptake rates and shorter turnover times of Fe observed at 300 m compared to 15 m, especially in the case of siderophore-bound Fe, resulting in higher uptake rates per cell and higher Fe : C ratios at depth. There are several experimental details and environmental factors that should be considered when interpreting these observations. For example, macronutrients are elevated at 300 m relative to 15 m, so it is possible Fe uptake rates were enhanced due to relief from macronutrient limitation. However, our surface water treatments included nitrate amendments that should have alleviated nitrogen limitation for at least some members of the microbial community. Organic carbon availability and lability also likely differed significantly between surface and mesopelagic waters, and would impact the observed Fe uptake and Fe : C ratios (Fourquez et al. 2020; Ratnarajah et al. 2021; Manck et al. 2024). The experiments at 300 m were also incubated at the same temperature as the 15 m experiments, likely enhancing the uptake rate of Fe relative to in situ rates due to increased metabolic activity at higher temperatures. However, it is not clear why this would stimulate uptake rates above those measured in surface waters. There might also be differences in the in-situ Fe bioavailability between the euphotic and mesopelagic zones, such as differences in colloidal Fe concentrations which can impact Fe availability. This might cause one population to respond more or less rapidly to an Fe addition, despite similar initial dissolved Fe concentrations. An additional possibility is that the ^{55}Fe adsorbed to the outside of cells or detritus more readily at 300 m, causing apparent high Fe uptake compared to 15 m. If this was the case, we would have expected the dead controls from 300 m to have significantly higher activities than those from 15 m, and this was not observed. Furthermore, oxalate rinsing was applied to all samples, which should remove most (if not all) adsorbed Fe. Finally, in terms of the observed Fe : C ratios, an additional source of uncertainty may come from the conversion of Fe uptake to Fe : C using a fixed carbon quota. Fe : C ratios based on a fixed carbon quota overlap with published values for surface waters, but resulted in values for 300 m that were significantly higher (Table S1). If the actual carbon quota per cell is significantly higher in heterotrophic bacteria at 300 m, then the calculated Fe : C ratios presented here could be artificially elevated. Cellular carbon estimates are not available for any cultured marine bacteria from mesopelagic waters, so we are not able to determine if this fixed carbon quota is too low.

Accounting for these factors, it is likely that the fast uptake rates and short turnover times of Fe observed at 300 m are related to differences in Fe acquisition by the microbial community at this depth, reflecting different metabolic strategies among organisms in the mesopelagic compared to the euphotic zone. The Fe requirements of heterotrophic bacteria are not well known, but evidence suggests they are elevated relative to large phytoplankton (Fe : C ~ 2.0 μmol : mol) or cyanobacteria (Fe : C ~ 19 μmol : mol) (Strzepek et al. 2005). Published estimates for heterotrophic bacteria Fe : C ratios range from 7.5 (Tortell et al. 1996) to 83 μmol : mol (Mazzotta et al. 2020), and the observations at 300 m in this study expand that range to upwards of 700 μmol : mol. The range of Fe requirements observed across these studies likely varies according to experimental growth conditions and the lifestyle strategies of specific groups of bacteria under consideration. In the current study, the 1 nmol L^{-1} dissolved Fe additions and slightly higher in situ dissolved Fe concentrations at 300 m may have supported luxury Fe uptake and storage by the in situ bacteria community. This could lead to higher Fe uptake at these depths, and much higher Fe : C quotas than for surface bacteria communities. Previous work has identified multiple copies of the Fe-storage protein bacterioferritin in a cultured marine heterotroph (Mazzotta et al. 2020) and modeling work suggests that bacteria competitively consume Fe and that Fe storage plays a large role (Ratnarajah et al. 2021). Alternatively, it

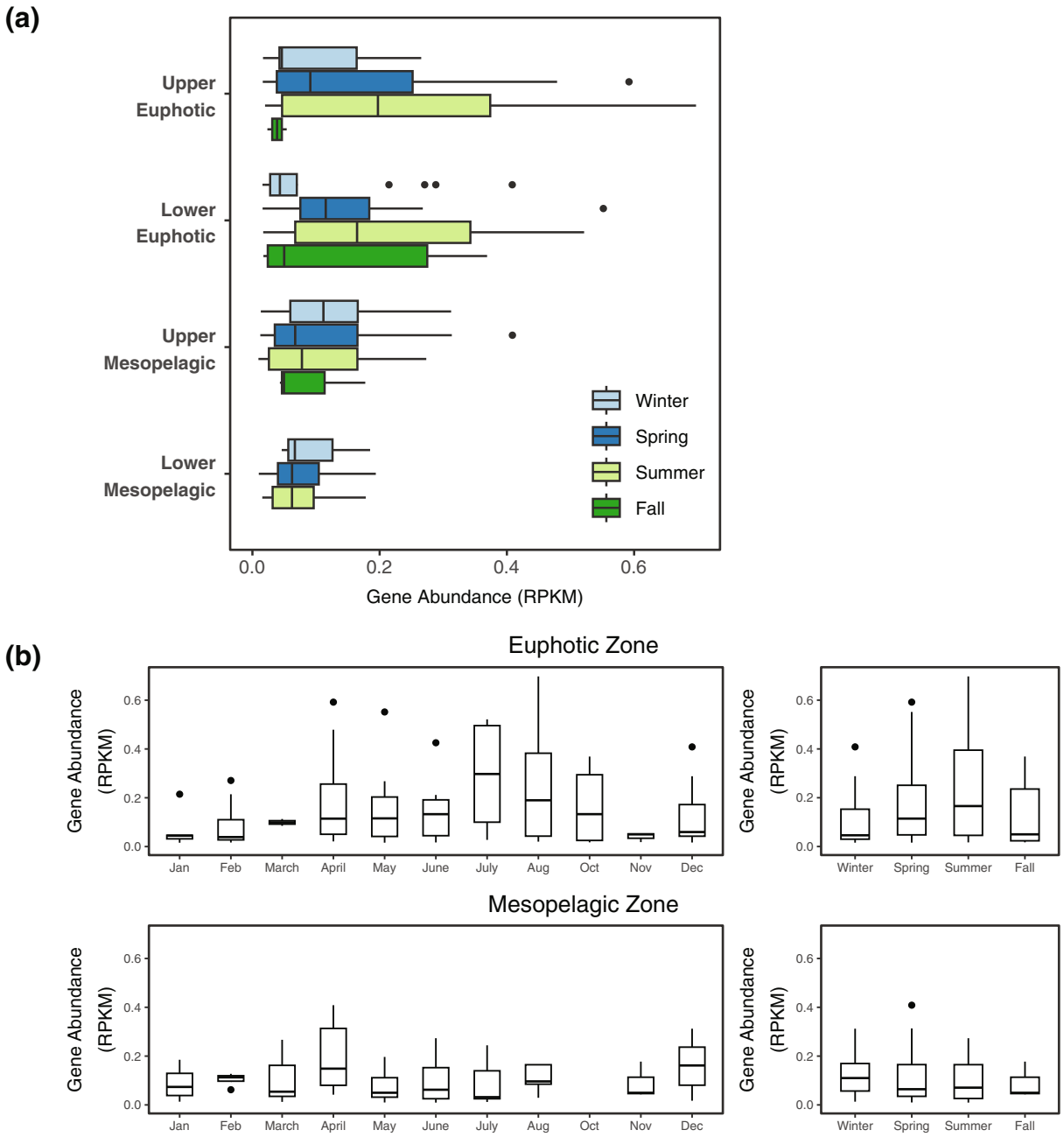

Fig. 5. Seasonal abundance of genes from siderophore biosynthetic gene clusters detected at Station ALOHA between May 2015–April 2016 plotted as reads per kilobase per million (RPKM). (**a**) Box plots display the interquartile range of gene abundances detected within a given depth range and season. Median values are plotted as solid vertical lines, and outliers are plotted as distinct points. Depth ranges are as follows: upper euphotic 0–75 m, lower euphotic > 75 to 150 m, upper mesopelagic > 150 to 300 m, mid-mesopelagic > 300 to 500 m. (**b**) Box plots display the interquartile range of gene abundances detected within a given month or season in the euphotic (0–150 m) and mesopelagic (150–500 m) zones. Median values are displayed as solid horizontal lines and outliers are plotted as distinct points. No data are available for September.

is possible that the consumption of the relatively refractory dissolved organic matter at these depths has a higher Fe requirement for marine bacteria, though this has not been explored to our knowledge. The energy-starved microbial community in the upper mesopelagic could have elevated metabolic requirements for Fe (Tortell et al. 1996) relative to the surface ocean community, potentially resulting from differences in the lability or oxidation state of organic matter. Additionally, nitrifying bacteria and archaea, whose cellular abundances significantly increase in mesopelagic waters, appear to have high Fe requirements (Shafiee et al. 2019; Saito et al. 2020). In addition to the high uptake rates and Fe : C

Table 1. Siderophores measured in the water column and siderophore biosynthetic gene clusters (BGCs) identified at Station ALOHA. Siderophores identified in the water column are grouped according to type and are shown in the table based on that grouping. For example, multiple different forms of amphibactins were detected (Table S2) but are all grouped here under "amphibactin." Specific siderophore IDs can be found in Table S2. The "–" denotes that the specific siderophore was not found either in the water column or in the Station ALOHA gene catalog.

Siderophore	Biosynthetic pathway	Siderophore type	Depth(s)	Season	BGC in gene catalog
Aerobactin	NIS	Hydroxamate	–	–	Yes
Amphibactins	NRPS	Hydroxamate	300–400	Summer	–
Anguibactin	NRPS	Mixed (hydroxamate/catecholate)	–	–	Yes
Enterobactin	NIS	Catecholate	–	–	Yes
Ferrioxamaine	NIS	Hydroxamate	15–400	Spring, summer, winter	–
Petrobactin	NIS	Mixed (carboxylate/catecholate)	15	Winter	Yes
Piscibactin	NRPS	Mixed (carboxylate/hydroxamate)	15	Winter	Yes
(Pseudo)alterobactin	NRPS	Mixed (carboxylate/catecholate)	15	Winter	Yes
Synechobactin	NRPS	Mixed (carboxylate/hydroxamate)	15, 150	Spring, summer, winter	–
Thalassosamide	NIS	Hydroxamate	–	–	Yes
Vanchrobactin	NRPS	Catecholate	–	–	Yes
Vibrioferrin	NIS	Carboxylate	15	Winter	Yes
Vibriobactin	NRPS	Catecholate	–	–	Yes

NIS, NRPS-independent siderophore; NRPS, non-ribosomal peptide synthetase.

quotas observed here, other lines of evidence are starting to point to an increased demand for Fe in the mesopelagic. For example, high concentrations of siderophores have been observed in the upper mesopelagic ocean, suggesting active Fe uptake at these depths (Bundy et al. 2018; Park et al. 2023; Li et al. 2024). Ultimately, understanding the Fe requirements of mesopelagic bacteria could have important implications for carbon and Fe cycling in the twilight zone.

Siderophore production at station ALOHA reflects seasonal variation in primary production and organic matter availability

The turnover times of siderophore bound Fe determined from the uptake experiments shed insight into the seasonal distributions of siderophores and biosynthetic gene clusters at Station ALOHA. Dissolved siderophore concentrations were greatest in the spring, summer, and fall but almost entirely absent or low in winter (Fig. 4). The turnover times of Fe bound to siderophores suggest their lifetime in the marine environment is on the order of weeks to months (Fig. 1c), which may help explain differences in siderophore concentrations between seasons. There was high variability in total dissolved siderophore concentrations and the identity of siderophores observed over the study period. Some of this variability may have been caused by factors related to method developments over time. For example, siderophore concentrations were relatively high during our only fall sampling period (2013), but these earliest samples were not analyzed by the optimized liquid chromatography-Orbitrap mass spectrometry method for siderophore identification (Table S2). Furthermore, collecting profile samples during this time was not possible, because of the high volumes of water that were needed (800 L). However, improvements to methodological sensitivity prior to sample collection in 2014 allowed for the sensitive detection and identification of several siderophores from the winter cruise in this year despite the relatively low concentrations that were observed (Table S2).

The dissolved siderophore distributions were notably higher in the spring, summer, and fall, even when only considering surface waters (Fig. 4). The elevated concentrations of dissolved siderophores in spring and summer were matched by a higher potential for the microbial community to biosynthesize siderophores during these seasons, particularly in the euphotic zone (Fig. 5). Of the 14 different types of siderophores identified using mass spectrometry or from gene pathways in the metagenomes, 5 were found in both (Table 1). The remaining compounds were either only found in the water column and not in the metagenomes (2 of the 14), or conversely, the biosynthesis genes were found (7 of the 14) but the compound was not identified in the water column samples. A wide structural diversity of siderophores has been detected using the solid phase extraction and liquid chromatography mass spectrometry techniques employed here (Boiteau et al. 2019), making it unlikely that specific siderophores escaped detection in the water column due to methodological bias. Therefore, the limited overlap in the dominant siderophores measured and the biosynthetic gene clusters identified suggests that either some compounds may be underestimated from metagenomic approaches, or that some siderophores cycle too rapidly to be observed in

measurable quantities. Further uptake studies examining the bioavailability of the siderophore groups dominant within the metagenomes, such as catecholate-type siderophores, will help to further explain these differences.

Seasonality in nutrient supply, productivity, and export have all been documented in the North Pacific subtropical gyre and Station ALOHA (Fitzsimmons et al. 2015; Hawco et al. 2021; Karl et al. 2021) and all impact microbial community structure and thus siderophore production. In the spring, primary production begins to increase at Station ALOHA (Figs. 2, 3). This is thought to be a result of increasing solar irradiance (Karl et al. 2021) and these changes are especially evident in the lower euphotic zone (Letelier et al. 2004, 2017; Figs. S1, S2). This springtime increase in productivity generally coincides with the peak in Fe delivery to this region (Fitzsimmons et al. 2015). During this time, Fe is delivered primarily via atmospheric dust deposition which introduces lithogenic Fe particles to the surface ocean. In this study, the highest concentrations of dissolved siderophores were observed in surface waters during the spring and coincided with increasing biosynthetic capacity in the euphotic zone (Figs. 4, 5). It is likely that siderophore secretion by heterotrophic bacteria at Station ALOHA during this time may help solubilize particulate Fe (Bundy et al. 2018) and to compete with other microorganisms for Fe (Boiteau et al. 2016) as the Fe demand of the microbial community begins to increase during these productive months. For example, ferrioxamines have been shown to be produced during the degradation of sinking (Velasquez et al. 2016) or suspended particles (Bundy et al. 2018), and high siderophore concentrations were observed in the North Pacific Transition Zone in a region of high dust inputs (Park et al. 2023). Based on the turnover times of siderophores with respect to biological uptake determined in surface waters in this study, siderophores produced in surface waters during these episodic events would then be expected to persist on seasonal timescales.

As primary production increases throughout the late spring, essential nutrients such as nitrate and dissolved Fe are consumed. During late summer, when the physical delivery of nitrate to the surface ocean is low, nitrogen fixation is an important source of nitrogen fueling primary productivity (Karl et al. 2021). Rates of nitrogen fixation peak in the late summer and early fall at Station ALOHA when warm, stratified waters select for the growth of nitrogen-fixing cyanobacteria (Böttjer et al. 2017). This late summer production is also associated with a large pulse of particulate carbon export that reaches the sea floor and is thought to be the result of diatom growth supported by nitrogen-fixing endosymbionts (Karl et al. 2012). As a result of increasing primary production and temperature, rates of heterotrophic bacterial production are also elevated by late summer at Station ALOHA (Viviani and Church 2017). However, during this period, dust delivery to the surface ocean decreases (Fitzsimmons et al. 2015). Thus, an increased Fe demand of the microbial community resulting from high rates of primary production, nitrogen fixation, and bacterial production coincides with low rates of Fe delivery and likely intensifies the competition for Fe throughout the euphotic zone as summer progresses. This has the potential to set up conditions favoring the production of siderophores by bacteria as a means to competitively acquire Fe or to retain or recycle Fe in the euphotic zone over longer timescales (Boyd et al. 2015; Hayes et al. 2015; Hawco et al. 2022).

In addition to dissolved siderophore concentrations, the genetic potential for siderophore biosynthesis also peaked during the summer months. A majority of the genera found to have siderophore biosynthetic gene clusters in this study, such as *Vibrio* and *Alteromonas*, contain known copiotrophic bacteria, suggesting that siderophore production may be common to heterotrophs responding to episodic inputs of organic matter during periods of elevated production (Fontanez et al. 2015; Pelve et al. 2017; Church et al. 2021). These genera have been found to be dominant in sediment trap material from Station ALOHA and association with sinking eukaryotes (Fontanez et al. 2015). Thus in many cases, siderophore production might largely be due to the Fe demand of heterotrophic bacteria as they consume carbon from sinking particles (Hopkinson and Barbeau 2012). In this study, seasonal patterns in the genetic potential for siderophore production within the euphotic zone closely followed those of the abundance of both suspended and sinking particles, further suggesting that siderophore biosynthesis may be directly tied to the dynamics of particle production. While the genetic potential for siderophore production did not vary seasonally in the mesopelagic zone, elevated dissolved siderophore concentrations were observed in the summer in this region of the water column, potentially in response to the elevated particle flux escaping the euphotic zone during this time. Given the faster turnover times of siderophores measured in this region of the water column ($\sim$ 1 month across all siderophore treatments), elevated siderophore concentrations persisting over the course of a season likely reflect ongoing siderophore production within mesopelagic waters. Finally, in winter, siderophore concentrations and the abundance of siderophore biosynthetic gene clusters were reduced significantly throughout the water column, likely reflecting the decrease in metabolic activity or Fe demand of heterotrophic bacteria as productivity and the availability of organic substrates diminished, or increased mixing that dilutes siderophores.

Together, the higher concentrations of siderophores from spring to fall and the dominance of copiotrophic bacteria identified as potential siderophore producers in the metagenomes, predict that siderophore production is heightened during periods of enhanced productivity at Station ALOHA and provides compelling evidence that ligand production by the microbial community plays an important role in the seasonal cycling and retention of Fe at Station ALOHA. Uptake rates of Fe in the euphotic zone agree with previous measurements at Station ALOHA and imply that Fe is cycled rapidly by the microbial community in this region. While less bioavailable than

inorganic Fe additions, siderophore-bound Fe proved to be a bioavailable source of Fe to the microbial community in both the euphotic and mesopelagic zones. Importantly, we found the resulting bioavailability depended on the specific siderophore structure, warranting additional studies focused on elucidating specific compounds in the Fe-binding ligand pool and their uptake kinetics in natural communities. Due to longer turnover times of Fe bound to siderophores, the production of strong siderophores has the potential to transform dissolved Fe into a form that persists in the water column on longer time scales. The finding that Fe uptake rates and turnover times were faster in the mesopelagic waters than in the surface ocean was surprising and merits further investigation. Such results suggest Fe availability is impacting microbial dynamics and Fe cycling at depth.

Data availability statement

Iron uptake data are available as Supporting Information and on Zenodo (DOI: 10.5281/zenodo.7062571). Sequence data are available from the NCBI short read archive (SRA) under Bioproject no. PRJNA352737.

References

Baars, O., F. M. M. Morel, and D. H. Perlman. 2014. ChelomEx: Isotope-assisted discovery of metal chelates in complex media using high-resolution LC–MS. Anal. Chem. **86**: 11298–11305. doi:10.1021/ac503000e

Barbeau, K. 2006. Photochemistry of organic iron(III) complexing ligands in oceanic systems. Photochem. Photobiol. **82**: 1505–1516. doi:10.1562/2006-06-16-ir-935

Boiteau, R. M., J. N. Fitzsimmons, D. J. Repeta, and E. A. Boyle. 2013. Detection of iron ligands in seawater and marine cyanobacteria cultures by high-performance liquid chromatography-inductively coupled plasma-mass spectrometry. Anal. Chem. **85**: 4357–4362. doi:10.1021/ac3034568

Boiteau, R. M., and others. 2016. Siderophore-based microbial adaptations to iron scarcity across the eastern Pacific Ocean. Proc. Natl. Acad. Sci. **113**: 14237–14242. doi:10.1073/pnas.1608594113

Boiteau, R. M., C. P. Till, T. H. Coale, J. N. Fitzsimmons, K. W. Bruland, and D. J. Repeta. 2019. Patterns of iron and siderophore distributions across the California current system. Limnol. Oceanogr. **64**: 376–389. doi:10.1002/lno.11046

Bolger, A. M., M. Lohse, and B. Usadel. 2014. Trimmomatic: A flexible trimmer for Illumina sequence data. Bioinformatics **30**: 2114–2120. doi:10.1093/bioinformatics/btu170

Böttjer, D., J. E. Dore, D. M. Karl, R. M. Letelier, C. Mahaffey, S. T. Wilson, J. Zehr, and M. J. Church. 2017. Temporal variability of nitrogen fixation and particulate nitrogen export at station ALOHA. Limnol. Oceanogr. **62**: 200–216. doi:10.1002/lno.10386

Boyd, P. W., R. F. Strzepek, M. J. Ellwood, D. A. Hutchins, S. D. Nodder, B. S. Twining, and S. W. Wilhelm. 2015. Why are biotic iron pools uniform across high- and low-iron pelagic ecosystems? Global Biogeochem. Cycles **29**: 1028–1043. doi:10.1002/2014gb005014

Bundy, R. M., R. M. Boiteau, C. McLean, K. A. Turk-Kubo, M. R. McIlvin, M. A. Saito, B. A. S. Van Mooy, and D. J. Repeta. 2018. Distinct Siderophores contribute to iron cycling in the mesopelagic at station ALOHA. Front. Mar. Sci. **5**: 1–15. doi:10.3389/fmars.2018.00061

Church, M. J., E. Kyi, R. O. Hall Jr., D. M. Karl, M. Lindh, A. Nelson, and E. K. Wear. 2021. Production and diversity of microorganisms associated with sinking particles in the subtropical North Pacific Ocean. Limnol. Oceanogr. **66**: 3255–3270. doi:10.1002/lno.11877

Cordero, O. X., L.-A. Ventouras, E. F. DeLong, and M. F. Polz. 2012. Public good dynamics drive evolution of iron acquisition strategies in natural bacterioplankton populations. Proc. Natl. Acad. Sci. **109**: 20059–20064. doi:10.1073/pnas.1213344109

DiTullio, G. R., and E. A. Laws. 1991. Impact of an atmospheric-oceanic disturbance on phytoplankton community dynamics in the North Pacific central gyre. Deep Sea Res. Part A. Oceanogr. Res. Pap. **38**: 1305–1329. doi:10.1016/0198-0149(91)90029-F

Dore, J. E., and D. M. Karl. 1996. Nitrite distributions and dynamics at station ALOHA. Deep Sea Res. Part II Top. Stud. Oceanogr. **43**: 385–402. doi:10.1016/0967-0645(95)00105-0

Dutkiewicz, S., A. E. Hickman, O. Jahn, W. W. Gregg, C. B. Mouw, and M. J. Follows. 2015. Capturing optically important constituents and properties in a marine biogeochemical and ecosystem model. Biogeosciences **12**: 4447–4481. doi:10.5194/bg-12-4447-2015

Eddy, S. R. 2011. Accelerated profile HMM searches. PLoS Comput. Biol. **7**: e1002195. doi:10.1371/journal.pcbi.1002195

Fitzsimmons, J. N., C. T. Hayes, S. N. Al-Subiai, R. Zhang, P. L. Morton, R. E. Weisend, F. Ascani, and E. A. Boyle. 2015. Daily to decadal variability of size-fractionated iron and iron-binding ligands at the Hawaii Ocean Time-series Station ALOHA. Geochim. Cosmochim. Acta **171**: 303–324. doi:10.1016/j.gca.2015.08.012

Fontanez, K. M., J. M. Eppley, T. J. Samo, D. M. Karl, and E. F. DeLong. 2015. Microbial community structure and function on sinking particles in the North Pacific subtropical gyre. Front. Microbiol. **6**: 469. doi:10.3389/fmicb.2015.00469

Foreman, R. K., M. Segura-Noguera, and D. M. Karl. 2016. Validation of Ti (III) as a reducing agent in the chemiluminescent determination of nitrate and nitrite in seawater. Mar. Chem. **186**: 83–89. doi:10.1016/j.marchem.2016.08.003

Fourquez, M., M. Bressac, S. L. Deppeler, M. Ellwood, I. Obernosterer, T. W. Trull, and P. W. Boyd. 2020. Microbial

competition in the subpolar Southern Ocean: An Fe–C co-limitation experiment. Front. Mar. Sci. **6**: 776. doi:10.3389/fmars.2019.00776

Gledhill, M., and K. N. Buck. 2012. The organic complexation of iron in the marine environment: A review. Front. Microbiol. **3**: 69. doi:10.3389/fmicb.2012.00069

Hawco, N. J., and others. 2021. Iron depletion in the deep chlorophyll maximum: Mesoscale eddies as natural iron fertilization experiments. Global Biogeochem. Cycles **35**: e2021GB007112. doi:10.1029/2021GB007112

Hawco, N. J., S.-C. Yang, P. Pinedo-González, E. E. Black, J. Kenyon, S. Ferrón, X. Bian, and S. G. John. 2022. Recycling of dissolved iron in the North Pacific subtropical gyre. Limnol. Oceanogr. **67**: 2448–2465. doi:10.1002/lno.12212

Hayes, C. T., J. N. Fitzsimmons, E. A. Boyle, D. McGee, R. F. Anderson, R. Weisend, and P. L. Morton. 2015. Thorium isotopes tracing the iron cycle at the Hawaii Ocean Time-series Station ALOHA. Geochim. Cosmochim. Acta **169**: 1–16. doi:10.1016/j.gca.2015.07.019

Hider, R. C., and X. Kong. 2010. Chemistry and biology of siderophores. Nat. Prod. Rep. **27**: 637–657. doi:10.1039/b906679a

Hogle, S. L., and others. 2022. Siderophores as an iron source for picocyanobacteria in deep chlorophyll maximum layers of the oligotrophic ocean. ISME J. **16**: 1636–1646. doi:10.1038/s41396-022-01215-w

Hopkinson, B. M., and K. A. Barbeau. 2012. Iron transporters in marine prokaryotic genomes and metagenomes. Environ. Microbiol. **14**: 114–128. doi:10.1111/j.1462-2920.2011.02539.x

Hopkinson, B., J. Nunnery, and K. Barbeau. 2005. Bioavailability and chemistry of iron(III)-porphyrin complexes. Abstr. Pap. Am. Chem. Soc. **229**: 075-GEOC.

Jones, D. R., D. M. Karl, and E. A. Laws. 1996. Growth rates and production of heterotrophic bacteria and phytoplankton in the North Pacific subtropical gyre. Deep Sea Res. Part I Oceanogr. Res. Pap. **43**: 1567–1580. doi:10.1016/S0967-0637(96)00079-9

Karl, D. M., and R. Lukas. 1996. The Hawaii Ocean time-series (HOT) program: Background, rationale and field implementation. Deep Sea Res. Part II Top. Stud. Oceanogr. **43**: 129–156. doi:10.1016/0967-0645(96)00005-7

Karl, D., R. Letelier, L. Tupas, and J. Dore. 1997. The role of nitrogen fixation in biogeochemical cycling in the subtropical North Pacific Ocean. Nature **388**: 533–538. doi:10.1038/41474

Karl, D. M., M. J. Church, J. E. Dore, R. M. Letelier, and C. Mahaffey. 2012. Predictable and efficient carbon sequestration in the North Pacific Ocean supported by symbiotic nitrogen fixation. Proc. Natl. Acad. Sci. **109**: 1842–1849. doi:10.1073/pnas.1120312109

Karl, D. M., R. M. Letelier, R. R. Bidigare, K. M. Björkman, M. J. Church, J. E. Dore, and A. E. White. 2021. Seasonal-to-decadal scale variability in primary production and particulate matter export at station ALOHA. Prog. Oceanogr. **195**: 102563. doi:10.1016/j.pocean.2021.102563

Kirchman, D. L. 2016. Growth rates of microbes in the oceans. Ann. Rev. Mar. Sci. **8**: 285–309. doi:10.1146/annurev-marine-122414-033938

Kramer, J., Ö. Özkaya, and R. Kümmerli. 2020. Bacterial siderophores in community and host interactions. Nat. Rev. Microbiol. **18**: 152–163. doi:10.1038/s41579-019-0284-4

Letelier, R. M., D. M. Karl, M. R. Abbott, and R. R. Bidigare. 2004. Light driven seasonal patterns of chlorophyll and nitrate in the lower euphotic zone of the North Pacific subtropical gyre. Limnol. Oceanogr. **49**: 508–519. doi:10.4319/lo.2004.49.2.0508

Letelier, R. M., A. E. White, R. R. Bidigare, B. Barone, M. J. Church, and D. M. Karl. 2017. Light absorption by phytoplankton in the North Pacific subtropical gyre. Limnol. Oceanogr. **62**: 1526–1540. doi:10.1002/lno.10515

Letelier, R. M., and others. 2019. Climate-driven oscillation of phosphorus and iron limitation in the North Pacific subtropical gyre. Proc. Natl. Acad. Sci. U. S. A. **116**: 12720–12728. doi:10.1073/pnas.1900789116

Li, H., and R. Durbin. 2009. Fast and accurate short read alignment with burrows–wheeler transform. Bioinformatics **25**: 1754–1760. doi:10.1093/bioinformatics/btp324

Li, J., and others. 2024. Microbial iron limitation in the ocean's twilight zone. Nature **633**: 823–827. doi:10.1038/s41586-024-07905-z

Liao, Y., G. K. Smyth, and W. Shi. 2014. featureCounts: An efficient general purpose program for assigning sequence reads to genomic features. Bioinformatics **30**: 923–930. doi:10.1093/bioinformatics/btt656

Lis, H., Y. Shaked, C. Kranzler, N. Keren, and F. M. M. Morel. 2015. Iron bioavailability to phytoplankton: An empirical approach. ISME J. **9**: 1003–1013. doi:10.1038/ismej.2014.199

Longhurst, A. R. 2010. Ecological geography of the sea. Elsevier.

Lory, C., and others. 2022. Assessing the contribution of diazotrophs to microbial Fe uptake using a group specific approach in the Western tropical South Pacific Ocean. ISME Commun. **2**: 41. doi:10.1038/s43705-022-00122-7

Luo, E., J. M. Eppley, A. E. Romano, D. R. Mende, and E. F. DeLong. 2020. Double-stranded DNA virioplankton dynamics and reproductive strategies in the oligotrophic open ocean water column. ISME J. **14**: 1304–1315. doi:10.1038/s41396-020-0604-8

Maldonado, M. T., and N. M. Price. 2001. Reduction and transport of organically bound iron by *Thalassiosira oceanica* (Bacillariophyceae). J. Phycol. **37**: 298–309. doi:10.1046/j.1529-8817.2001.037002298.x

Manck, L. E., J. Park, B. J. Tully, A. M. Poire, R. M. Bundy, C. L. Dupont, and K. A. Barbeau. 2022. Petrobactin, a siderophore produced by *Alteromonas*, mediates community iron acquisition in the global ocean. ISME J. **16**: 358–369. doi:10.1038/s41396-021-01065-y

Manck, L. E., T. H. Coale, B. M. Stephens, K. O. Forsch, L. I. Aluwihare, C. L. Dupont, A. E. Allen, and K. A. Barbeau. 2024. Iron limitation of heterotrophic bacteria in the California current system tracks relative availability of organic carbon and iron. ISME J. **18**: wrae061. doi:10.1093/ismejo/wrae061

Mawji, E., and others. 2008. Hydroxamate siderophores: Occurance and importance in the Atlantic Ocean. Environ. Sci. Technol. **42**: 8675–8680. doi:10.1021/es801884r

Mazzotta, M. G., M. R. McIlvin, and M. A. Saito. 2020. Characterization of the Fe metalloproteome of a ubiquitous marine heterotroph, *Pseudoalteromonas* (BB2-AT2): Multiple bacterioferritin copies enable significant Fe storage. Metallomics **12**: 654–667. doi:10.1039/d0mt00034e

Medema, M. H., and others. 2011. antiSMASH: Rapid identification, annotation and analysis of secondary metabolite biosynthesis gene clusters in bacterial and fungal genome sequences. Nucleic Acids Res. **39**: W339–W346. doi:10.1093/nar/gkr466

Mende, D. R., J. A. Bryant, F. O. Aylward, J. M. Eppley, T. Nielsen, D. M. Karl, and E. F. DeLong. 2017. Environmental drivers of a microbial genomic transition zone in the ocean's interior. Nat. Microbiol. **2**: 1367–1373. doi:10.1038/s41564-017-0008-3

Park, J., and others. 2023. Siderophore production and utilization by marine bacteria in the North Pacific Ocean. Limnol. Oceanogr. **68**: 1636–1653. doi:10.1002/lno.12373

Pelve, E. A., K. M. Fontanez, and E. F. DeLong. 2017. Bacterial succession on sinking particles in the ocean's interior. Front. Microbiol. **8**: 2269. doi:10.3389/fmicb.2017.02269

Pinedo-González, P., and others. 2020. Anthropogenic Asian aerosols provide Fe to the North Pacific Ocean. Proc. Natl. Acad. Sci. U. S. A. **117**: 27862–27868. doi:10.1073/pnas.2010315117

Ratnarajah, L., S. Blain, P. W. Boyd, M. Fourquez, I. Obernosterer, and A. Tagliabue. 2021. Resource colimitation drives competition between phytoplankton and bacteria in the Southern Ocean. Geophys. Res. Lett. **48**: 1–11. doi:10.1029/2020GL088369

Saito, M. A., and others. 2020. Abundant nitrite-oxidizing metalloenzymes in the mesopelagic zone of the tropical Pacific Ocean. Nat. Geosci. **13**: 355–362. doi:10.1038/s41561-020-0565-6

Salmon, T. P., A. L. Rose, B. A. Neilan, and T. D. Waite. 2006. The FeL model of iron acquisition: Nondissociative reduction of ferric complexes in the marine environment. Limnol. Oceanogr. **51**: 1744–1754. doi:10.4319/lo.2006.51.4.1744

Sandy, M., and A. Butler. 2009. Microbial iron acquisition: Marine and terrestrial siderophores. Chem. Rev. **109**: 4580–4595. doi:10.1021/cr9002787

Shafiee, R. T., J. T. Snow, Q. Zhang, and R. E. M. Rickaby. 2019. Iron requirements and uptake strategies of the globally abundant marine ammonia-oxidising archaeon, *Nitrosopumilus maritimus* SCM1. ISME J. **13**: 2295–2305. doi:10.1038/s41396-019-0434-8

Shaked, Y., and H. Lis. 2012. Disassembling iron availability to phytoplankton. Front. Microbiol. **3**: 123. doi:10.3389/fmicb.2012.00123

Smith, D. C., and F. Azam. 1992. A simple, economical method for measuring bacterial protein synthesis rates in seawater using 3H-leucine. Mar. Microb. Food Webs **6**: 107–114.

Strzepek, R. F., M. T. Maldonado, J. L. Higgins, J. Hall, K. Safi, S. W. Wilhelm, and P. W. Boyd. 2005. Spinning the "ferrous wheel": The importance of the microbial community in an iron budget during the FeCycle experiment. Global Biogeochem. Cycles **19**: GB4S26. doi:10.1029/2005GB002490

Sutak, R., J.-M. Camadro, and E. Lesuisse. 2020. Iron uptake mechanisms in marine phytoplankton. Front. Microbiol. **11**: 566691. doi:10.3389/fmicb.2020.566691

Tagliabue, A., and others. 2016. How well do global ocean biogeochemistry models simulate dissolved iron distributions? Global Biogeochem. Cycles **30**: 149–174. doi:10.1002/2015gb005289

Tortell, P. D., M. T. Maldonado, and N. M. Price. 1996. The role of heterotrophic bacteria in iron-limited ocean ecosystems. Lett. Nat. **383**: 330–332. doi:10.1038/383330a0

Tortell, P. D., M. T. Maldonado, J. Granger, and N. M. Priece. 1999. Marine bacteria and geochemical cycling of iron in the oceans. FEMS Microbiol. Ecol. **29**: 1–11. doi:10.1111/j.1574-6941.1999.tb00593.x

Tovar-Sanchez, a. 2003. A trace metal clean reagent to remove surface-bound iron from marine phytoplankton. Mar. Chem. **82**: 91–99. doi:10.1016/S0304-4203(03)00054-9

Velasquez, I. B., E. Ibisanmi, E. W. Maas, P. W. Boyd, S. Nodder, and S. G. Sander. 2016. Ferrioxamine siderophores detected amongst iron binding ligands produced during the remineralization of marine particles. Front. Mar. Sci. **3**: 172. doi:10.3389/fmars.2016.00172

Viviani, D. A., and M. J. Church. 2017. Decoupling between bacterial production and primary production over multiple time scales in the North Pacific subtropical gyre. Deep Sea Res. Part I Oceanogr. Res. Pap. **121**: 132–142. doi:10.1016/j.dsr.2017.01.006

Vraspir, J. M., and A. Butler. 2009. Chemistry of marine ligands and siderophores. Ann. Rev. Mar. Sci. **1**: 43–63. doi:10.1146/annurev.marine.010908.163712

Acknowledgments

Special thanks to the Captain and crew of the R/V *Kilo Moana* and R/V *Ka'imikai-O-Kanaloa* for help with sample collection, to the Hawaii Ocean Time-series program for the numerous biogeochemical measurements, and to Kendra A. Turk-Kubo for additional flow cytometry analyses. We would also like to thank Travis Mellett and two anonymous reviewers for

their helpful comments on the manuscript. RM Bundy was funded by a Life Sciences-Simons Early Career Investigator in Marine Microbial Ecology and Evolution Awards (Award 618401) and a Woods Hole Oceanographic Institution postdoctoral fellowship. RM Boiteau was funded by a Simons Early Career Investigator in Marine Microbial Ecology and Evolution Award (Award 621513). LEM was funded by a Simons Postdoctoral Fellowship in Marine Microbial Ecology (Award 729162). MJC was funded by the Simons Collaboration on Ocean Processes (Award 721221). NJH was supported by Life Sciences-Simons Early Career Investigator in Marine Microbial Ecology and Evolution Awards (Award 924096).

Conflict of Interest

None declared.

Submitted 29 March 2024
Revised 23 August 2024
Accepted 04 November 2024

Associate Editor: Katherina Petrou